Catal Lett (2016) 146:1544–1551
DOI 10.1007/s10562-016-1788-4

Catalytic Oxidation of CO Over $LaMn_{1-x}B_xO_3$ (B = Cu, Fe) Perovskite-type Oxides

Ali Tarjomannejad[1] · Aligholi Niaei[1] · Ali Farzi[1] · Dariush Salari[2] · Parisa Rashidi Zonouz[3]

Received: 26 May 2016 / Accepted: 5 June 2016 / Published online: 15 June 2016

Abstract In this paper, catalytic oxidation of CO over perovskite-type oxides $LaMn_{1-x}B_xO_3$ (B = Cu, Fe and x = 0, 0.1, 0.3, 0.5) were investigated. The perovskite catalysts were synthesized by sol–gel method and characterized by XRD, BET, H_2-TPR, XPS and SEM. XRD patterns showed that the samples are single-phase perovskite. By introduction of Cu and Fe in the structure, Specific surface area of $LaMnO_3$ was decreased, but the reducibility and oxygen vacancy were increased. The synthesized perovskite catalysts show high activity for the CO oxidation. Substitution of Mn by Cu and Fe enhanced the catalytic activity. The cu-containing perovskites showed a higher activity in CO oxidation compared with Fe-containing perovskites. The $LaMn_{0.7}Cu_{0.3}O_3$ perovskite showed the highest activity among the synthesized perovskites (T50 and T90 % of 110 and 142 °C). The excellent activity of $LaMn_{0.7}B_{0.3}O_3$ was associated to reducibility at low temperature, more oxygen vacancies and synergistic effect between Cu and Mn. The apparent activation energies were obtained and $LaMn_{0.7}Cu_{0.3}O_3$ as the most active catalyst, has the least activation energy compared with other synthesized catalysts.

Graphical Abstract

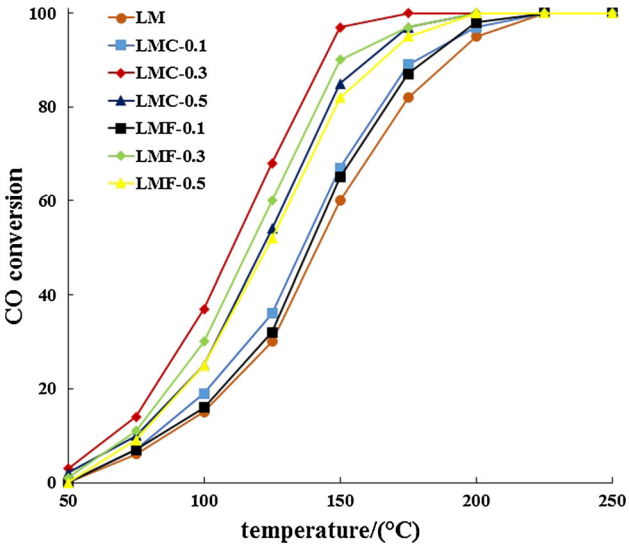

Keywords $LaMn_{1-x}B_xO_3$ · CO oxidation · Perovskite · Activation energy

1 Introduction

Carbon monoxide is one of the main gaseous pollutants, which is generally released from the combustion of fossil fuel in diesel engines. There are many methods for removal of CO including adsorption, thermal elimination and catalytic oxidation. Catalytic oxidation of CO is proved to be one of the most efficient techniques to remove this pollutant [1, 2]. Present catalysts are supported noble metal catalysts based on platinum, palladium, and rhodium [3, 4]. High cost, low stability and lack of noble metal limit their applications.

✉ Aligholi Niaei
aniaei@tabrizu.ac.ir

[1] Department of Chemical & Petroleum Engineering, University of Tabriz, Tabriz, Iran

[2] Department of Applied Chemistry, Faculty of Chemistry, University of Tabriz, Tabriz, Iran

[3] Faculty of Engineering, Tehran North Branch, Islamic Azad University, Tehran, Iran

Perovskite-type oxides are interesting catalysts for CO oxidation. They have lower cost and higher thermal stability than supported noble catalysts [5, 6].

The general formula ABO_3 is related to perovskite-type oxides which can crystallise in cubic structure [7]. A and B are two cations of very different sizes which must meet the so called tolerance factor tolerance factor $(0.8 < t < 1.0)$ defined by the equation $t = (r_A + r_O)/\sqrt{2}(r_B + r_O)$, where r_A, r_B and r_O are the ionic radii for A, B and O, respectively [8].

In mentioned structure coordination number with oxygen anions is 12 and 6 for A and B cation respectively. These catalysts have the capability to incorporate different cation types in their A-site and B-site leading to different compounds with general formula $A_{1-x}A'_xB_{1-x}B'_xO_3$ [9, 10]. Rare earth, alkaline earth and alkali metal cations are usually in A site which are larger in comparison to transition metal cations which are common occupant of B-site [11]. In perovskite-type oxides catalytic properties mainly depends on the nature of A and B ions and on their valence state [12, 13].

Perovskites with lanthanum in A-site exhibit higher activity in comparison to other formulations for catalytic oxidation of CO. First series transition metals are the most common metals for B-site [14–16]. Among the perovskite-type oxides, manganese containing perovskite catalysts has attracted more attention for CO oxidation as they are active in a wide range of reactions for transformation of carbon monoxide [17–19]. Copper and iron were generally regarded as an active cation for CO oxidation [14, 19]. So, by incorporation of these cations into the B-site of the perovskite structure a good performance can be achieved.

In this paper, effects of substitution of Mn by Cu and Fe in B-site of perovskites on chemical–physical properties and activity of catalysts were investigated. For this aim, a series of perovskite-type oxides $LaMn_{1-x}B_xO_3$ (B = Cu, Fe and x = 0, 0.1, 0.3, 0.5) were prepared by sol–gel method and characterized by XRD, BET, H_2-TPR, XPS and SEM. The catalytic performances of prepared catalysts were investigated for the CO oxidation at temperature ranges of 50–250 °C.

2 Experimental

2.1 Catalyst Preparation

$LaMn_{1-x}B_xO_3$ perovskite catalysts were prepared by the sol–gel method starting from $La(NO_3)_3{\cdot}6H_2O$, $Cu(NO_3)_2{\cdot}3H_2O$, $Fe(NO_3)_3{\cdot}9H_2O$, $Mn(NO_3)_2{\cdot}4H_2O$ and Citric acid monohydrate. For preparation of 1 g of catalyst, appropriate amount of La, Mn and B nitrates with cation ratios of La:Mn:B, of 1:1−x:x were dissolved in 50 mL of de-ionized water. Citric acid monohydrate is added to the solution of the cations with a molar ratio of 1:0.525 with respect to the total amount of cations. Then the solution was heated up to 80 °C with stirring until a sticky gel was obtained. The gel is heated to 200 °C for 2 h in air to remove the organic ligands and decompose the nitrates and turned into a dark powder and then calcined at 700 °C for 5 h in static air.

2.2 Characterizations

X-ray diffraction (XRD) patterns of perovskite catalysts were recorded on an X-ray diffractometer (D-500, SIEMENS) with a Kα line of copper (λ = 0.154 nm). Measurements of the samples were collected in the 2θ range of 20–80°. The Specific surface areas (m^2/g) of the perovskite catalysts was determined by nitrogen adsorption–desorption porosimetry at 77 K using an Autosorb-1 Quantachrome analyzer. Temperature programmed reduction (TPR) experiments were carried out in a Micromeritics Autochem 2900. The H_2-TPR experiments were performed with a 5 % H_2/Ar gas flow at 20 standard cubic centimeters per minute (sccm) and linear heating rate of 10 °C/min at 40–950 °C. X-ray photoelectron spectroscopy (XPS) measurements were performed to evaluate surface composition and oxidation state of perovskite catalysts over a Microlab 310-F scanning microprobe spectrometer with AlKα X-ray source (E = 1486 eV). The morphology of the synthesized particles was observed by scanning electron microscopy (SEM) using a Tescan instrument.

2.3 Catalytic Activity

The activities of perovskite catalysts were evaluated using a quartz tubular reactor with an internal diameter of 9 mm and length of 600 mm under atmospheric pressure and at different temperatures (50–250 °C). The reactant gas (1 % CO, 20 % O_2 and Ar as balance) was passed through 200 mg of catalysts at a rate of 100 mL/min ($GHSV = 6000^{-1}$). The powder sample were inserted into the middle of a quartz tube. The reactor was heated with an electrical furnace. The catalytic activities were tested under steady state conditions. The gas composition was analyzed before and after the reaction by an online gas chromatograph (Shimadzu 2010) equipped with a HP-Molesieve column (l = 30 m, i.d. = 0.53 mm) and thermal conductivity detector (TCD).

3 Results and Discussion

Figure 1 shows the XRD patterns of $LaMn_{1-x}B_xO_3$ perovskite samples. A comparison of XRD patterns with the pattern of $LaMnO_3$ (ICSD 082315) indicated that catalysts

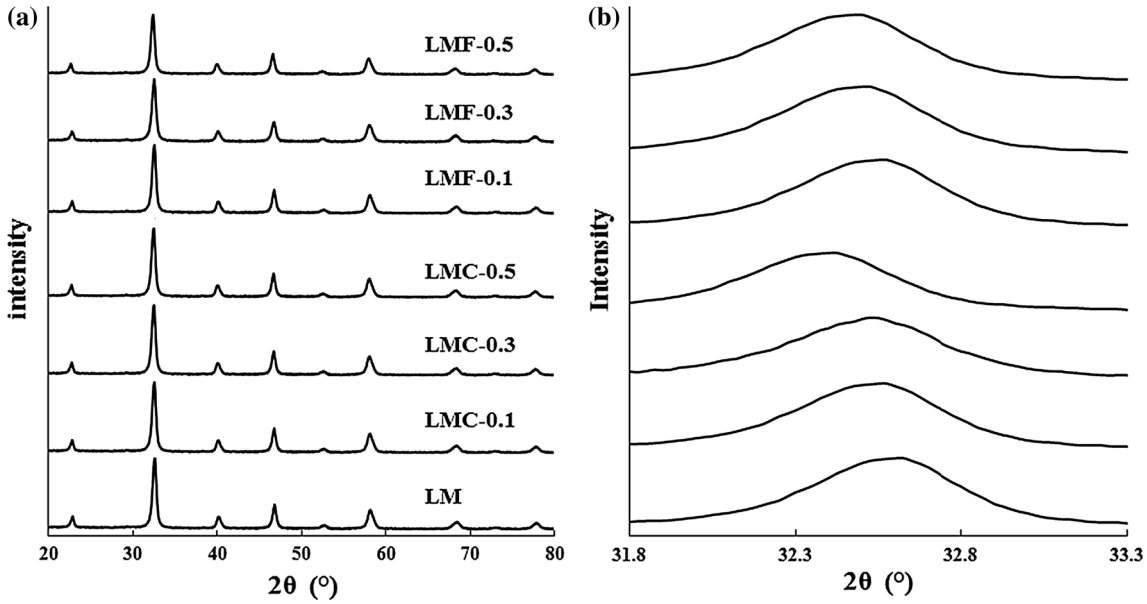

Fig. 1 XRD patterns of $LaMn_{1-x}B_xO_3$ perovskite samples

were single-phase perovskite oxides. There were no additional peaks corresponding to secondary phases or starting materials in XRD pattern of perovskites, suggesting that cupper and iron metals are completely dissolved in the perovskite structure. It appears that doping of cupper and iron to the structure doesn't change in the peak shape or intensity significantly. By introduction of Fe and Mn, no segregation phase was observed in the perovskites. In the section b of Fig. 1 by 2θ comparison of the catalysts main peak, it is revealed that main peak of each catalyst was observed in shifted 2θ which is a result of modifier metal insertion in the $LaMnO_3$ structure and change of the unit cell size.

BET surface area of perovskites was listed in Table 1. BET surface area values of perovskites are between 27 and 40 m^2/g; introduction of B cations causes the decrease in the specific surface area. The same results were observed in the literate [10, 20].

The reducibility of $LaMnO_3$ and $LaMn_{0.7}B_{0.3}O_3$ perovskite catalysts was investigated by H_2-TPR. Figure 2 shows the H_2-TPR curves of perovskite catalysts. It can be

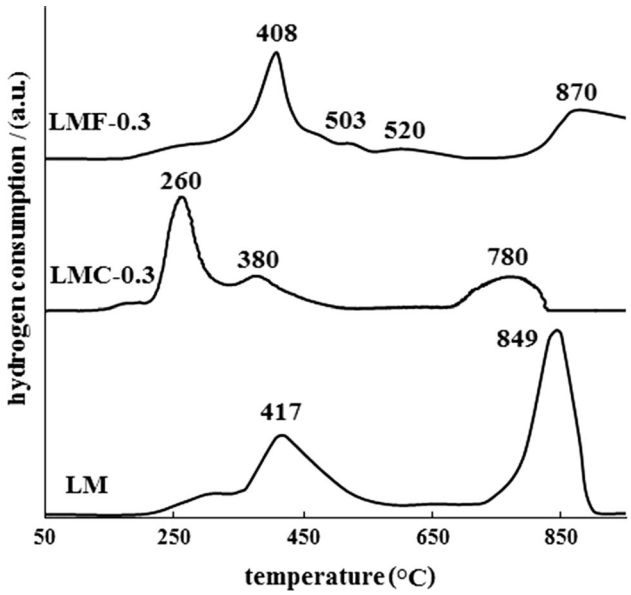

Fig. 2 H_2-TPR curves of perovskite samples

Table 1 Specific surface area, T50 %, T100 % and activation energies of perovskite samples

Catalyst	BET (m^2/g)	T50 % (°C)	T90 % (°C)	Activation energy (kJ/mol)
$LaMnO_3$	40	141	188	39.8
$LaMn_{0.9}Cu_{0.1}O_3$	36	136	176	36.9
$LaMn_{0.7}Cu_{0.3}O_3$	34	110	142	32.2
$LaMn_{0.5}Cu_{0.5}O_3$	29	122	157	35.9
$LaMn_{0.9}Fe_{0.1}O_3$	33	139	180	37.9
$LaMn_{0.7}Fe_{0.3}O_3$	31	116	150	34.1
$LaMn_{0.5}Fe_{0.5}O_3$	27	124	162	36.6

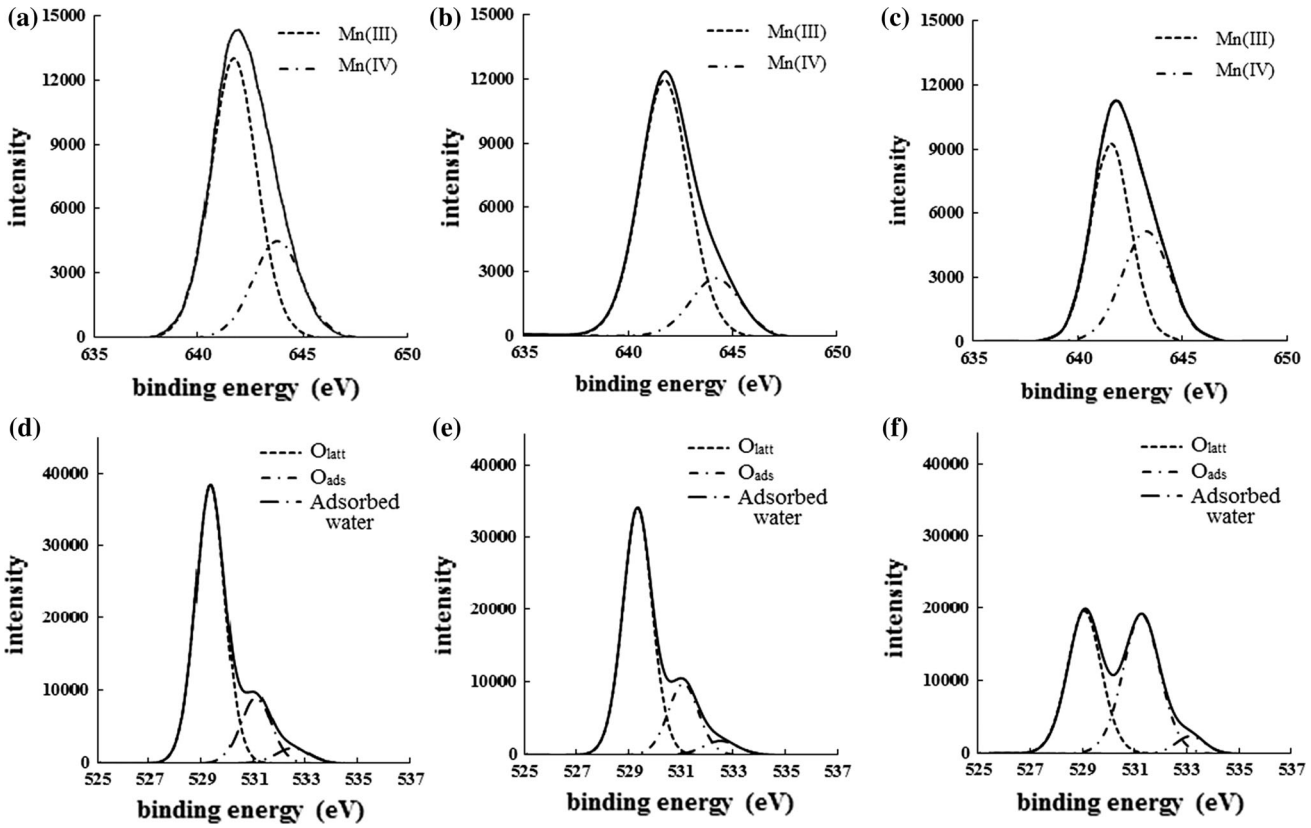

Fig. 3 XPS spectra of perovskite samples, Mn $2p_{3/2}$ of (**a**) $LaMnO_3$, (**b**) $LaMn_{0.7}Cu_{0.3}O_3$, (**c**) $LaMn_{0.7}Fe_{0.3}O_3$, O 1 s of (**d**) $LaMnO_3$, (**e**) $LaMn_{0.7}Cu_{0.3}O_3$, (**f**) $LaMn_{0.7}Fe_{0.3}O_3$

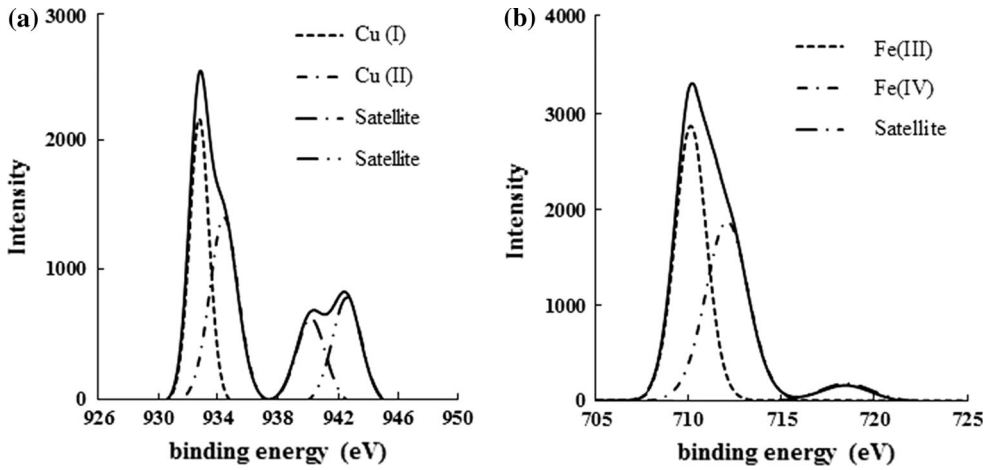

Fig. 4 XPS spectra of perovskite samples. (**a**) Cu $2p_{3/2}$ of $LaMn_{0.7}Cu_{0.3}O_3$, (**b**) Fe $2p_{3/2}$ of $LaMn_{0.7}Fe_{0.3}O_3$

seen that the $LaMnO_3$ shows two signal peaks at 417 and 849 °C, which has been associated to the reduction of Mn^{4+} to Mn^{3+} and Mn^{3+} to Mn^{2+}, respectively [17, 21, 22]. But for the catalysts partially substituted by Fe, they display four signal peaks at 408, 520, 603 and 870 °C [22, 23]. The first and forth signal peaks are related to the reduction of Mn^{4+} and Mn^{3+} presented in the perovskite, but the others should be come from the reduction of Fe^{4+} to Fe^{3+} and Fe^{3+} to Fe^{2+}. Fe^{2+} can be reduced to Fe^0, but this reduction occurs under temperature higher than 1000 °C. So, for reduction of Iron, two peaks including reduction of Fe^{4+} to Fe^{3+} and Fe^{3+} to Fe^{2+} are exist.

In the TPR profile of $LaMn_{0.7}Cu_{0.3}O_3$, The first signal peaks are also related to the reduction of Cu^{2+} to Cu^0, but the

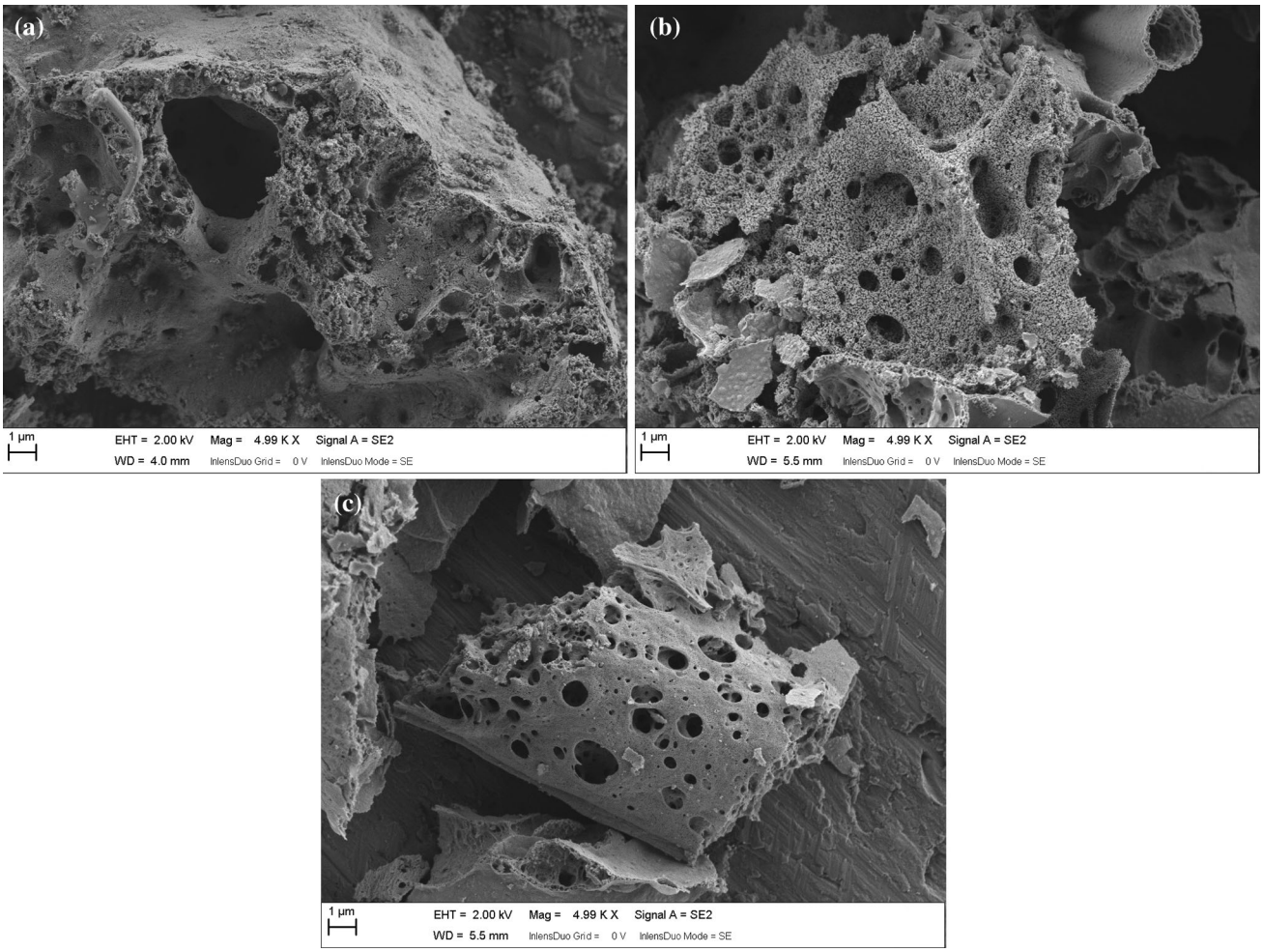

Fig. 5 SEM images of perovskite samples, (**a**) $LaMnO_3$, (**b**) $LaMn_{0.7}Cu_{0.3}O_3$, (**c**) $LaMn_{0.7}Fe_{0.3}O_3$

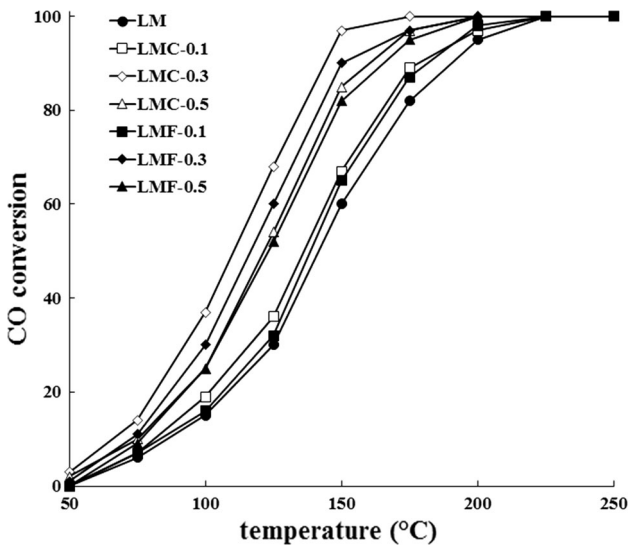

Fig. 6 Catalytic Oxidation of CO over $LaMn_{1-x}B_xO_3$ perovskite samples

others assigned to the reduction of Mn^{4+} and Mn^{3+}. When compared the reduction peaks of Mn^{4+} of $LaMn_{0.7}B_{0.3}O_3$ with $LaMnO_3$, this peak shifts to lower temperature especially the reduction peak of $LaMn_{0.7}Cu_{0.3}O_3$ at 380 °C. These results indicate that the Mn–O bond strength can be weakened by the substitution of the B-site elements with copper and iron.

The surface composition of $LaMnO_3$ and $LaMn_{0.7}B_{0.3}O_3$ perovskites was investigated by XPS. The XPS spectra for Mn $2p_{3/2}$ of LaMnO3 and $LaMn_{0.7}B_{0.3}O_3$ perovskites are shown in Fig. 3. The Mn $2p_{3/2}$ spectra includes two peaks correspond to Mn^{3+} (641.5 eV) and Mn^{4+} (644 eV) [24–26]. Mn in all the samples consists of both Mn^{4+} and Mn^{3+} ions. By substitution of Mn by copper, the ratio of Mn^{4+} to Mn^{3+} was decreased. But, by substitution by iron, this ratio was increased. The XPS spectra for Cu $2p_{3/2}$ and Fe $2p_{3/2}$ of $LaMn_{0.7}B_{0.3}O_3$ are shown in Fig. 4. In Cu $2p_{3/2}$ spectrum, two peaks at the binding energies of 531.2 and

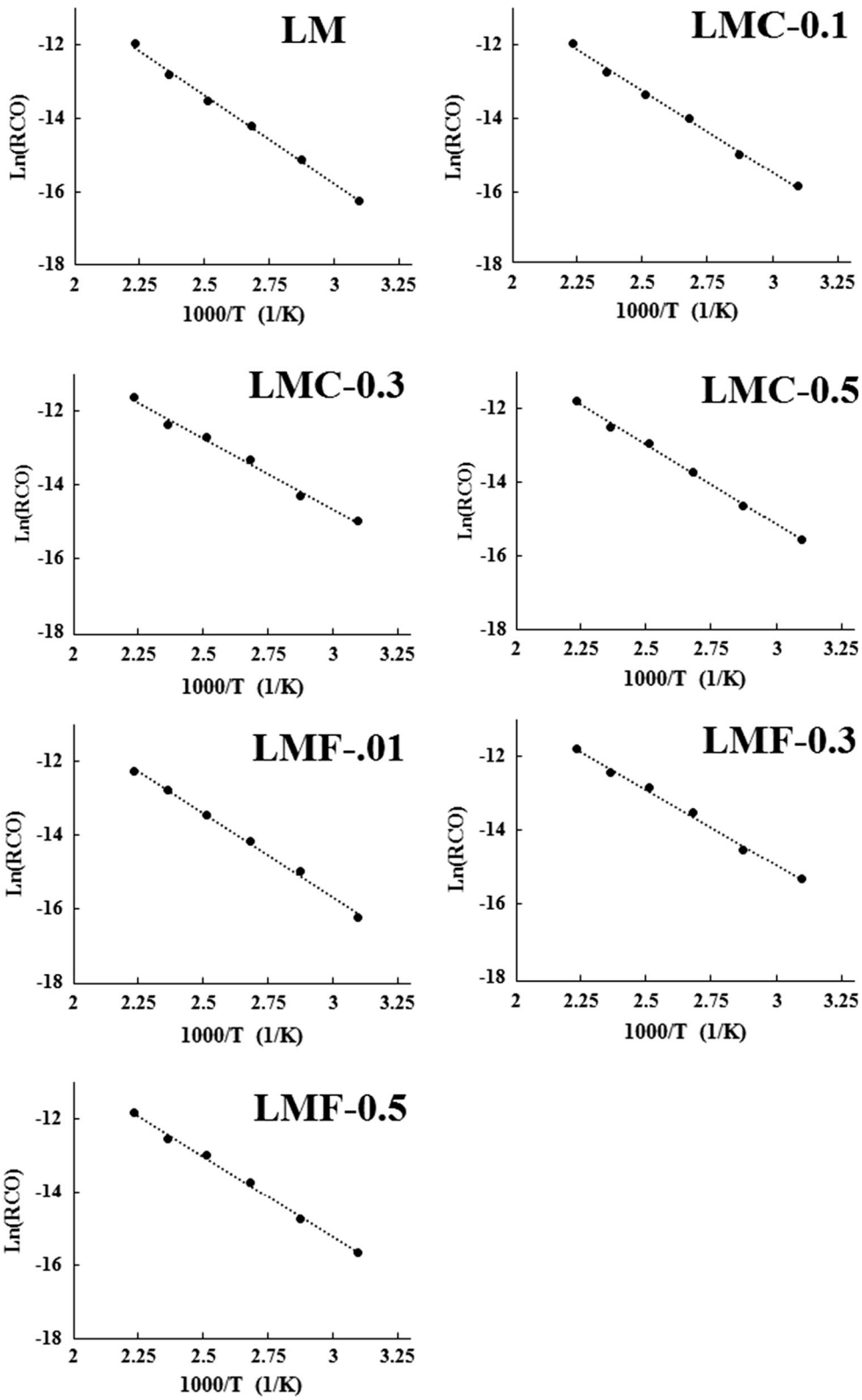

Fig. 7 The Arrhenius plots for perovskite samples

533.4 eV correspond to Cu^{1+} and Cu^{2+} ions [27–29]. Fe $2p_{3/2}$ spectrum includes three peaks correspond to Fe^{3+} (710.1 eV), Fe^{4+} (712.1 eV) and a satellite [14, 24, 30].

The XPS spectra for O 1 s of the samples are also shown in Fig. 3. In O 1 s spectrum, three peaks at the binding energies of 529.5, 531.1, and 533.1 eV can be

assigned to lattice oxygen (O_{latt}), adsorbed oxygen (O_{ads}), and surface adsorbed water species, respectively [14, 24, 25]. Generally, the adsorb oxygen concentration is related to the oxygen vacancy concentration [31]. Substitution of La and Mn by other cations can result in the formation of oxygen vacancies and thereby causing a decrease in the lattice oxygen concentration. It can be seen from Fig. 3, by substitution of Mn by copper and iron, the ratio of O_{ads}/O_{latt} was increased. This result means that more oxygen vacancies were produced in the perovskite structure in the doped samples.

The morphology and particle size of synthesized perovskite catalysts were investigated by SEM. SEM images of perovskites are shown in Fig. 5. Morphology of perovskites was as irregular shaped grains.

Figure 6 shows the temperature profile for CO conversion over $LaMn_{1-x}B_xO_3$ perovskite catalysts. At these conditions, all the B-doped perovskite catalysts reach an almost complete conversion at 225 °C. Temperatures for 50 and 90 % conversion of CO (T50 and T90 %) for all catalysts are shown in Table 1. By considering the T50 and T90 % of CO conversion as criteria of activity, Cu-containing perovskite catalysts showed a higher activity than Fe-containing perovskites. Results indicate that the conversion was in order of L-MC-0.3 > L-MF-0.3 > L-MC-0.5 > L-MF-0.5 > L-MC-0.1 > L-MF-0.1 > L-M.

Catalytic activity of perovskites for CO oxidation depends on reducibility of transition metal cations, oxidation state of ions, oxygen vacancy concentration and specific surface area. Substitution of Mn by other cations in the perovskite reduced the reduction temperature of manganese and increased the reducibility of perovskites [32]. The ratio of Mn^{4+}/Mn^{3+} was changed by substitution of manganese and this factor can cause structural defects in perovskite structure. Introduction of Cations in B-site increased the ratio of O_{ads}/O_{latt} and increased the oxygen vacancy concentration on the surface of perovskite [23, 33]. High reducibility, more structural defects and oxygen vacancies lead to higher catalytic activity and an improvement in perovskite performance. There is no direct relationship was observed between specific surface area and catalytic activity. Therefore, it is concluded that the excellent catalytic activity of $LaMn_{0.7}Cu_{0.3}O_3$ is associated with high reduction ability, oxygen vacancies and more structural defects in its structure.

Reaction rates (rates of CO oxidation) were evaluated from the Eq. 1:

$$R_{CO} = \frac{F_{CO0}X_{CO}}{W_{cat}} \quad (1)$$

Where R_{CO} is the rate of CO oxidation (mol/(s.gr_{cat})), F_{CO0} is the molar flow rate of CO (mol/s), X_{CO} is the CO conversion and W_{cat} is the weight of catalyst by grams. Arrhenius-type plots of the form $\ln(R_{CO}) = f(1000/T)$ for perovskites are shown in Fig. 7, where R is the rate of conversion (mol/(g s)). As observed from these figures, there is a straight-line and from its slope the apparent activation energy can be estimated. Activation energies of synthesized perovskite for CO oxidation were listed in Table 1. Substitution of manganese by copper and iron, reduces the apparent activation energy to 32.2 kJ/mol from 39.2 kJ/mol in $LaMnO_3$. The lower apparent activation energy coincides with the observed increase in catalytic activity. $LaMn_{0.7}Cu_{0.3}O_3$ which has the lowest activation energy (32.2 kJ/mol), was also found to be the most active catalyst in the synthesized perovskites and $LaMnO_3$ has the highest activation energy (39.2 kJ/mol). The values of activation energies do not show sensible changes with B cations and x value and remain in the range $32.2 < E_{app} < 39.2$ kJ/kmol. Chan et al. [20] found the apparent activation energy of $La_{1-x}Sr_xMnO_3$ perovskites between 48.3 and 66 kJ/kmol. Wang et al. [34] calculated activation energy of $LaSrNiO_4$ equals to 49.3 kJ/mol. Variation of activation energy with introduction of cations in A or B site is small. These values are compared satisfactorily with the values calculated in this work.

4 Conclusions

Catalytic activity of $LaMn_{1-x}B_xO_3$ (B = Cu, Fe and x = 0, 0.1, 0.3, 0.5) obtained by sol–gel method evaluated in CO oxidation and characterized by XRD, BET, H_2-TPR, XPS and SEM. Pure perovskite crystal phases are achieved by sol–gel method and no segregation phase was observed in the perovskite structure. Specific surface areas of perovskites were obtained in the range of 27–40 m^2/g. $LaMn_{1-x}B_xO_3$ perovskites proved quite active for CO oxidation. Substitution of manganese by copper and iron in the perovskite increased the reduction ability and oxygen vacancy concentration of perovskite catalysts. Based on results, Cu-containing perovskite catalysts have a higher activity than Fe-containing perovskite catalysts. $LaMn_{0.7}Cu_{0.3}O_3$ perovskite catalyst showed the highest activity (90 % at 142 °C) among the studied $LaMn_{1-x}B_xO_3$ perovskites for CO conversion. Nearly complete elimination of CO was achieved at 150 °C with this catalyst. The excellent catalytic activity of $LaMn_{0.7}Cu_{0.3}O_3$ is associated with the absence of segregation phase, high reduction ability, reduction Mn^{4+} in lower temperature, oxygen vacancies and more structural defects in its structure. Apparent activation energies for synthesized perovskites were obtained from Arrhenius-type plots confirmed that the $LaMn_{0.7}Cu_{0.3}O_3$ has the lowest activation energy (32.2 kJ/mol) compared with other synthesized catalysts.

References

1. Ladas S, Poppa H, Boudart M (1981) Surf Sci 102:151–171
2. Tang X, Hao J, Li J (2009) Front Environ Sci Eng China 3:265–270
3. Libby W (1971) Science 171:499–500
4. Voorhoeve R, Johnson D, Remeika J, Gallagher P (1977) Science 195:827–833
5. Singh UG, Li J, Bennett JW, Rappe AM, Seshadri R, Scott SL (2007) J Catal 249:349–358
6. Pena M, Fierro J (2001) Chem Rev 101:1981–2018
7. Stathopoulos VN, Belessi VC, Bakas TV, Neophytides SG, Costa CN, Pomonis PJ, Efstathiou AM (2009) Appl Catal B Environ 93:1–11
8. Cimino S, Lisi L, De Rossi S, Faticanti M, Porta P (2003) Appl Catal B Environ 43:397–406
9. Khanfekr A, Arzani K, Nemati A, Hosseini M (2009) Int J Environ Sci Technol 6:105–112
10. Yan X, Huang Q, Li B, Xu X, Chen Y, Zhu S, Shen S (2013) J Ind Eng Chem 19:561–565
11. Keav S, Matam SK, Ferri D, Weidenkaff A (2014) Catalysts 4:226–255
12. Song K-S, Cui HX, Kim SD, Kang S-K (1999) Catal Today 47:155–160
13. Izadkhah B, Niaei A, Salari D, Hosseinpoor S, Hosseini SA, Tarjomannejad A (2015) Korean J Chem Eng 33:1192–1199
14. Gao B, Deng J, Liu Y, Zhao Z, Li X, Wang Y, Dai H (2013) Chin J Catal 34:2223–2229
15. Tascon J, Tejuca LG (1980) React Kinet Catal Lett 15:185–191
16. George S, Viswanathan B (1983) React Kinet Catal Lett 22:411–415
17. Abdolrahmani M, Parvari M, Habibpoor M (2010) Chin J Catal 31:394–403
18. Li R, Ma J, Xu J, Zhou X, Su Z (2000) React Kinet Catal Lett 70:363–370
19. Tien-Thao N, Alamdari H, Kaliaguine S (2008) J Solid State Chem 181:2006–2019
20. Chan K, Ma J, Jaenicke S, Chuah G, Lee J (1994) Appl Catal A Gen 107:201–227
21. Hosseini SA, Salari D, Niaei A, Oskoui SA (2013) J Ind Eng Chem 19:1903–1909
22. Meiqing S, Zhen Z, Jiahao C, Yugeng S, Jun W, Xinquan W (2013) J Rare Earths 31:119–123
23. Oskoui SA, Niaei A, Tseng H-H, Salari D, Izadkhah B, Hosseini SA (2013) ACS comb sci 15:609–621
24. Yoon JS, Lim Y-S, Choi BH, Hwang HJ (2014) Int J Hydrog Energy 39:7955–7962
25. Zhan H, Li F, Xin C, Zhao N, Xiao F, Wei W, Sun Y (2015) Catal Lett 145:1177–1185
26. Zhong H, Zeng R (2006) J Serb Chem Soc 71:1049–1059
27. Cano E, Torres C, Bastidas J (2001) Mater Corros 52:667
28. Maluf S, Assaf E (2010) J Nat Gas Chem 19:567–574
29. Jo M, Tanaka A (1996) Appl Surf Sci 100:11–14
30. Tanaka H, Mizuno N, Misono M (2003) Appl Catal A Gen 244:371–382
31. Zheng S, Hua Q, Gu W, Liu B (2014) J Mol Catal A Chem 391:7–11
32. Yu Z, Gao L, Yuan S, Wu Y (1992) J Chem Soc Faraday Trans 88:3245–3249
33. Tanaka H, Misono M (2001) Curr Opin Solid State Mater Sci 5:381–387
34. Wang K, Zhong P (2010) J Serb Chem Soc 75:249–258